

1 **Temporal variability and driving factors of the carbonate system in the Aransas**
2 **Ship Channel, TX, USA: A time-series study**

3

4 **Melissa R. McCutcheon¹, Hongming Yao^{1,#}, Cory J. Staryk¹, Xinping Hu¹**

5 ¹ Harte Research Institute for Gulf of Mexico Studies, Texas A&M University – Corpus
6 Christi, TX 78412, USA

7 [#] current address: Shenzhen Engineering Laboratory of Ocean Environmental Big Data
8 Analysis and Application, Shenzhen Institute of Advanced Technology, Chinese
9 Academy of Sciences, Shenzhen 518055, China

10

11

12 *Correspondence to:* Melissa R. McCutcheon (melissa.mccutcheon@tamucc.edu)

13

14

15 **Keywords:** *p*CO₂, acidification, diel variability, seasonal variability, autonomous sensors

16 **Abstract**

17 The coastal ocean is affected by an array of co-occurring biogeochemical and
18 anthropogenic processes, resulting in substantial heterogeneity in water chemistry,
19 including carbonate chemistry parameters such as pH and partial pressure of CO₂ (*p*CO₂).
20 To better understand coastal and estuarine acidification and air-sea CO₂ fluxes, it is
21 important to study baseline variability and driving factors of carbonate chemistry. Using
22 both discrete bottle sample collection (2014-2020) and hourly sensor measurements
23 (2016-2017), we explored temporal variability, from diel to interannual scales, in the
24 carbonate system (specifically pH and *p*CO₂) at the Aransas Ship Channel located in
25 northwestern Gulf of Mexico. Using other co-located environmental sensors, we also
26 explored the driving factors of that variability. Both sampling methods demonstrated
27 significant seasonal variability at the location, with highest pH (lowest *p*CO₂) in the
28 winter and lowest pH (highest *p*CO₂) in the summer. Significant diel variability was also
29 evident from sensor data, but the time of day with elevated *p*CO₂/depressed pH was not
30 consistent across the entire monitoring period, sometimes reversing from what would be
31 expected from a biological signal. Though seasonal and diel fluctuations were smaller
32 than many other areas previously studied, carbonate chemistry parameters were among
33 the most important environmental parameters to distinguish between time of day and
34 between seasons. It is evident that temperature, biological activity, freshwater inflow, and
35 tide level (despite the small tidal range) are all important controls on the system, with
36 different controls dominating at different time scales. The results suggest that the
37 controlling factors of the carbonate system may not be exerted equally on both pH and
38 *p*CO₂ on diel timescales, causing separation of their diel or tidal relationships during

39 certain seasons. Despite known temporal variability on shorter timescales, discrete
40 sampling was generally representative of the average carbonate system and average air-
41 sea CO₂ flux on a seasonal and annual basis when compared with sensor data.

42 **1. Introduction**

43 Coastal waters, especially estuaries, experience substantial spatial and temporal
44 heterogeneity in water chemistry—including carbonate chemistry parameters such as pH
45 and partial pressure of CO₂ (*p*CO₂)—due to the diversity of co-occurring biogeochemical
46 and anthropogenic processes (Hofmann et al., 2011; Waldbusser and Salisbury, 2014).
47 Carbonate chemistry is important because an addition of CO₂ acidifies seawater, and
48 acidification can negatively affect marine organisms (Barton et al., 2015; Bednaršek et
49 al., 2012; Ekstrom et al., 2015; Gazeau et al., 2007; Gobler and Talmage, 2014).
50 Additionally, despite the small surface area of coastal waters relative to the global ocean,
51 coastal waters are recognized as important contributors in global carbon cycling (Borges,
52 2005; Cai, 2011; Laruelle et al., 2018).

53 While carbonate chemistry, acidification, and air-sea CO₂ fluxes are relatively
54 well studied and understood in open ocean environments, large uncertainties remain in
55 coastal environments. Estuaries are especially challenging to fully understand because of
56 the heterogeneity between and within estuaries that is driven by diverse processes
57 operating on different time scales such as river discharge, nutrient and organic matter
58 loading, stratification, and coastal upwelling (Jiang et al., 2013; Mathis et al., 2012). The
59 traditional sampling method for carbonate system characterization involving discrete
60 water sample collection and laboratory analysis is known to lead to biases in average
61 *p*CO₂ and CO₂ flux calculations due to daytime sampling that neglects to capture diel

62 variability (Li et al., 2018). Mean diel ranges in pH can exceed 0.1 unit in many coastal
63 environments, and especially high diel ranges (even exceeding 1 pH unit) have been
64 reported in biologically productive areas or areas with higher mean $p\text{CO}_2$ (Challener et
65 al., 2016; Cyronak et al., 2018; Schulz and Riebesell, 2013; Semesi et al., 2009; Yates et
66 al., 2007). These diel ranges can far surpass the magnitude of the changes in open ocean
67 surface waters that have occurred since the start of the industrial revolution and rival
68 spatial variability in productive systems, indicating their importance for a full
69 understanding of the carbonate system.

70 Despite the need for high-frequency measurements, sensor deployments have
71 been limited in estuarine environments (especially compared to their extensive use in the
72 open ocean) because of the challenges associated with highly variable salinities,
73 biofouling, and sensor drift (Sastri et al., 2019). Carbonate chemistry monitoring in the
74 Gulf of Mexico (GOM), has been relatively minimal compared to the United States east
75 and west coasts. The GOM estuaries currently have less exposure to concerning levels of
76 acidification than other estuaries because of their high temperatures (causing water to
77 hold less CO_2 and support high productivity year-round) and often suitable river
78 chemistries (i.e., relatively high buffer capacity) (McCutcheon et al., 2019; Yao et al.,
79 2020). However, respiration-induced acidification is present in both the open GOM (e. g.,
80 subsurface water influenced by the Mississippi River Plume and outer shelf region near
81 the Flower Garden Banks National Marine Sanctuary) and GOM estuaries, and most
82 estuaries in the northwestern GOM have also experienced long-term acidification (Cai et
83 al., 2011; Hu et al., 2018, 2015; Kealoha et al., 2020; McCutcheon et al., 2019; Robbins
84 and Lisle, 2018). This evidence of acidification as well as the relatively high CO_2 efflux

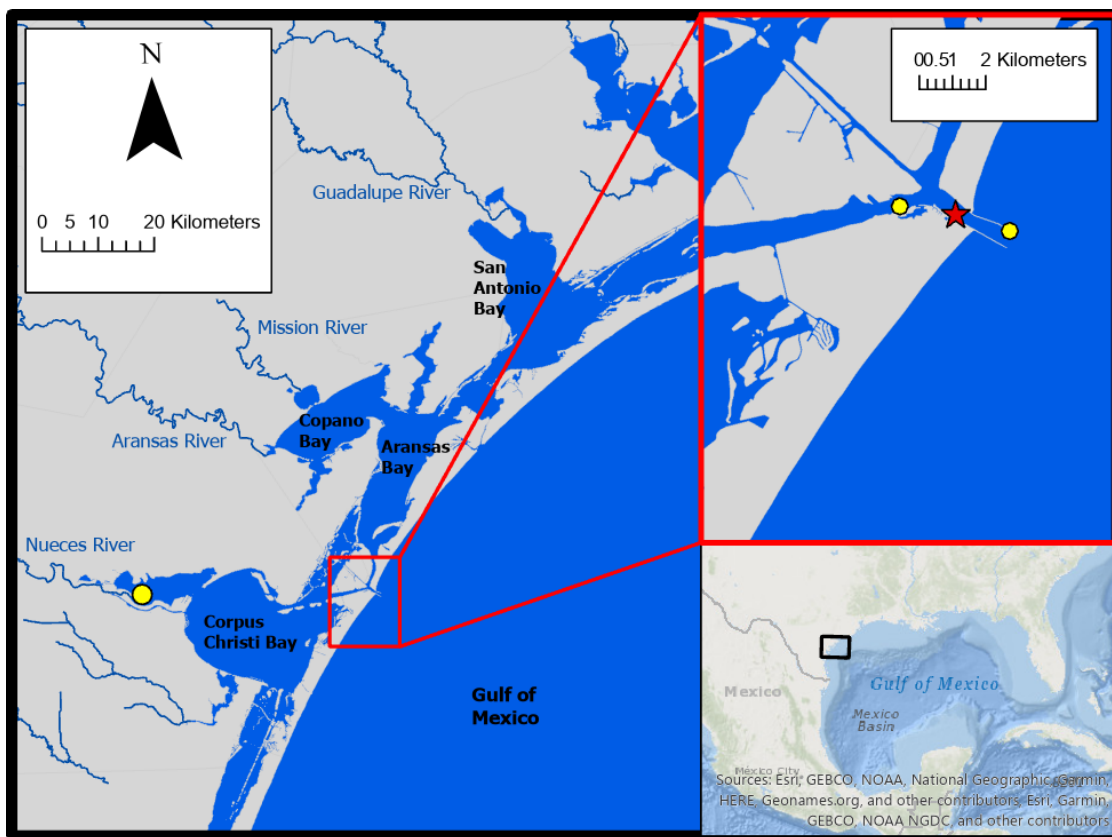
85 from the estuaries of the northwest GOM illustrates the necessity to study the baseline
86 variability and driving factors of carbonate chemistry in the region. In this study, we
87 explored temporal variability in the carbonate system in Aransas Ship Channel (ASC)—a
88 tidal inlet where the lagoonal estuaries meet the coastal waters in a semi-arid region of
89 the northwestern GOM—using both discrete bottle sample collection and hourly sensor
90 measurements, and we explored the driving factors of that variability using data from
91 other co-located environmental sensors. The characterization of carbonate chemistry and
92 consideration of regional drivers can provide context to acidification and its impacts and
93 improved estimates of air-sea CO₂ fluxes.

94 **2. Materials and Methods**

95 *2.1 Location*

96 Autonomous sensor monitoring and discrete water sample collections for
97 laboratory analysis of carbonate system parameters were performed in ASC (located at
98 27°50'17"N, 97°3'1"W). ASC is one of the few permanent tidal inlets that intersect a
99 string of barrier islands and connect the GOM coastal waters with the lagoonal estuaries
100 in the northwest GOM (Fig. 1). ASC provides the direct connection between the
101 northwestern GOM and the Mission-Aransas Estuary (Copano and Aransas Bays) to the
102 north and Nueces Estuary (Nueces and Corpus Christi Bays) to the south (Fig. 1). The
103 region is microtidal, with a small tidal range relative to many other estuaries, ranging
104 from ~ 0.6 m tides on the open coast to less than 0.3 m in upper estuaries (Montagna et
105 al., 2011). Mission-Aransas Estuary (MAE) is fed by two small rivers, the Mission (1787
106 km² drainage basin) and Aransas (640 km² drainage basin) Rivers
107 (<http://waterdata.usgs.gov/>), which both experience low base flows punctuated by

108 periodic high flows during storm events. MAE has an average residence time of one year
109 (Solis and Powell, 1999), so there is a substantial lag between time of rainfall and
110 riverine delivery to ASC in the lower estuary. A significant portion of riverine water
111 flowing into Aransas Bay originates from the larger rivers further northeast on the Texas
112 coast via the Intracoastal Waterway (i.e., Guadalupe River (26,625 km² drainage basin)
113 feeds San Antonio Bay and has a much shorter residence time of nearly 50 days) (Solis
114 and Powell, 1999; USGS, 2001).



115
116 **Figure 1.** Study area. The location of monitoring in the Aransas Ship Channel (red star)
117 and the locations of NOAA stations used for wind data (yellow circles) are shown.

118
119 *2.2 Continuous Monitoring*

120 Autonomous sensor monitoring (referred to throughout as continuous monitoring)
121 of pH and $p\text{CO}_2$ was conducted from Nov. 8, 2016 to Aug. 23, 2017 at the University of

122 Texas Marine Science Institute's research pier in ASC. Hourly pH data were collected
123 using an SAtlantic[®] SeaFET pH sensor (on total pH scale) and hourly $p\text{CO}_2$ data were
124 collected using a Sunburst[®] SAMI- CO_2 . The pH and $p\text{CO}_2$ sensors were placed in a
125 flowthrough system that received surface water from ASC using a time-controlled
126 diaphragm pump prior to each measurement. Hourly temperature and salinity data were
127 measured by a YSI[®] 600OMS V2 sonde. All hourly data were single measurements taken
128 on the hour. The average difference between sensor pH and discrete quality assurance
129 samples measured spectrophotometrically in the lab was used to establish a correction
130 factor (-0.05) across the entire sensor pH dataset. Note, this correction scheme was not
131 ideal (Bresnahan et al., 2014) although less rigorous correction based on sensor and
132 discrete pH values has also been used (Shadwick et al. 2019). Nevertheless, the overall
133 good agreement between discrete and corresponding sensor pH values during the
134 deployment period suggested that the SeaFET sensor remained stable. It is also worth
135 noting that our monitoring setup remained free from biofouling during the 10-month
136 period. We attribute this to the deployment design in which the high frequency movement
137 of the pumping mechanisms in the diaphragm pump must have eliminated the influence
138 of animal larvae. See supplemental materials for additional sensor deployment and
139 quality assurance information.

140 *2.3 Discrete Sample Collection and Sample Analysis*

141 Long-term monitoring via discrete water sample collection was conducted at ASC
142 from May 2, 2014 to February 25, 2020 (in addition to the discrete, quality assurance
143 sample collections). A single, discrete, surface water sample was collected every two
144 weeks during the summer months and monthly during the winter months from a small

145 vessel at a station near (<20 m from) the sensor deployment. Water sample collection
146 followed standard protocol for ocean carbonate chemistry studies (Dickson et al., 2007).
147 Ground glass borosilicate bottles (250 mL) were filled with surface water and preserved
148 with 100 μ L saturated mercury chloride (HgCl_2). Apiezon[®] grease was applied to the
149 bottle stopper, which was then secured to the bottle using a rubber band and a nylon hose
150 clamp.

151 These samples were used for laboratory dissolved inorganic carbon (DIC) and pH
152 measurements. DIC was measured by injecting 0.5 mL of sample into 1 ml 10% H_3PO_4
153 (balanced by 0.5 M NaCl) with a high-precision Kloehn syringe pump. The CO_2 gas
154 produced through sample acidification was then stripped using high-purity nitrogen gas
155 and carried into a Li-Cor infrared gas detector. DIC analyses had a precision of 0.1%.
156 Certified Reference Material (CRM) was used to ensure the accuracy of the analysis
157 (Dickson et al. 2003). For samples with salinity>20, pH was measured using a
158 spectrophotometric method at $25 \pm 0.1^\circ\text{C}$ (Carter et al. 2003) and the Douglas and Byrne
159 (2017) equation. Analytical precision of the spectrophotometric method for pH
160 measurement was ± 0.0004 pH units. A calibrated Orion Ross glass pH electrode was
161 used to measure pH at $25 \pm 0.1^\circ\text{C}$ for samples with salinity<20, and analytical precision
162 was ± 0.01 pH units. All pH values obtained using the potentiometric method were
163 converted to total scale at *in situ* temperature (Millero 2001). Salinity of the discrete
164 samples was measured using a benchtop salinometer calibrated by MilliQ water and a
165 known salinity CRM. For discrete samples, $p\text{CO}_2$ was calculated in CO2Sys for Excel
166 using laboratory-measured salinity, DIC, pH, and *in situ* temperature for calculations.
167 Carbonate speciation calculations were done using Millero (2010) carbonic acid

168 dissociation constants (K_1 and K_2), Dickson (1990) bisulfate dissociation constant, and
169 Uppström (1974) borate concentration.

170 *2.4 Calculation of CO₂ fluxes*

171 Equation 1 was used for air-water CO₂ flux calculations (Wanninkhof, 1992;
172 Wanninkhof et al., 2009). Positive flux values indicate CO₂ emission from the water into
173 the atmosphere (the estuary acting as a source of CO₂), and negative flux values indicate
174 CO₂ uptake by the water (the estuary acting as a sink for CO₂).

$$175 F = k K_0 (pCO_{2,w} - pCO_{2,a}) \quad (1)$$

176 where k is the gas transfer velocity (in $m\ d^{-1}$), K_0 (in $mol\ l^{-1}\ atm^{-1}$) is the solubility
177 constant of CO₂ (Weiss, 1974), and $pCO_{2,w}$ and $pCO_{2,a}$ are the partial pressure of CO₂ (in
178 μatm) in the water and air, respectively.

179 We used the wind speed parameterization for gas transfer velocity (k) from Jiang
180 et al. (2008) converted from $cm\ h^{-1}$ to $m\ d^{-1}$, which is thought to be the best estuarine
181 parameterization at this time (Crosswell et al., 2017), as it is a composite of k over
182 several estuaries. The calculation of k requires a windspeed at 10 m above the surface, so
183 windspeeds measured at 3 m above the surface were converted using the power law wind
184 profile (Hsu, 1994; Yao and Hu, 2017). To assess uncertainty, other parameterizations
185 with direct applications to estuaries in the literature were also used to calculate CO₂ flux
186 (Raymond and Cole 2001; Ho et al. 2006). We note that parameterization of k based on
187 solely windspeed is flawed because several additional parameters can contribute to
188 turbulence including turbidity, bottom-driven turbulence, water-side thermal convection,
189 tidal currents, and fetch (Wanninkhof 1992, Abril et al., 2009, Ho et al., 2104, Andersson

190 et al., 2017), however it is currently the best option for this system given the limited
191 investigations of CO₂ flux and contributing factors in estuaries.

192 Hourly averaged windspeed data for use in CO₂ flux calculations were retrieved
193 from the NOAA-controlled Texas Coastal Ocean Observation Network (TCOON;
194 <https://tidesandcurrents.noaa.gov/tcoon.html>). Windspeed data from the nearest TCOON
195 station (Port Aransas Station – located directly in ASC, < 2 km inshore from our
196 monitoring location) was prioritized when data were available. During periods of missing
197 windspeed data at the Port Aransas Station, wind speed data from TCOON’s Aransas
198 Pass Station (< 2 km offshore from monitoring location) were next used, and for all
199 subsequent gaps, data from TCOON’s Nueces Bay Station (~ 40 km away) were used
200 (Fig. 1; additional discussion of flux calculation and windspeed data can be found in
201 supplementary materials). For flux calculations from continuous monitoring data, each
202 hourly measurement of *p*CO₂ was paired with the corresponding hourly averaged
203 windspeed. For flux calculations from discrete sample data, the *p*CO₂ calculated for each
204 sampled day was paired with the corresponding daily averaged windspeed (calculated
205 from the retrieved hourly averaged windspeeds).

206 Monthly mean atmospheric xCO₂ data (later converted to *p*CO₂) for flux
207 calculations were obtained from NOAA’s flask sampling network of the Global
208 Monitoring Division of the Earth System Research Laboratory at the Key Biscayne (FL,
209 USA) station. Global averages of atmospheric xCO₂ were used when Key Biscayne data
210 were unavailable. Each *p*CO₂ observation (whether using continuous or discrete data)
211 was paired with the corresponding monthly averaged xCO₂ for flux calculations.
212 Additional information and justification are available in supplemental materials.

213 *2.5 Additional data retrieval and data processing to investigate carbonate system*
214 *variability and controls*

215 All reported annual mean values are seasonally weighted to account for
216 disproportional sampling between seasons. However, reported annual standard deviation
217 is associated with the un-weighted, arithmetic mean (Table S1). Temporal variability was
218 investigated in the form of seasonal and diel variability (Tables S1, S2, S3). For seasonal
219 analysis, December to February was considered winter, March to May was considered
220 spring, June to August was considered summer, and September to November was
221 considered fall. It is important to note that the Fall season had much fewer continuous
222 sensor observations than other seasons because of the timing of sensor deployment. For
223 diel comparisons, daytime and nighttime variables were defined as 09:00-15:00 local
224 standard time and 21:00-03:00 local standard time, respectively, based on the 6-hour
225 periods with highest and lowest photosynthetically active radiation (PAR; data from co-
226 located sensor, obtained from the Mission-Aransas National Estuarine Research Reserve
227 (MANERR) at <https://missionaransas.org/science/download-data>). Diel ranges in
228 parameters were calculated (daily maximum minus daily minimum) and only reported for
229 days with the full 24 hours of hourly measurements (176 out of 262 measured days) to
230 ensure that data gaps did not influence the diel ranges (Table S3).

231 Controls on $p\text{CO}_2$ from thermal and non-thermal (i.e., combination of physical
232 and biological) processes were investigated following Takahashi et al. (2002) over
233 annual, seasonal, and daily time scales using both continuous and discrete data. Over any
234 given time period, this method uses the ratio of the ranges of temperature-normalized
235 $p\text{CO}_2$ ($p\text{CO}_{2,\text{nt}}$, Eq. 2) and the mean annual $p\text{CO}_2$ perturbed by the difference between

236 mean and observed temperature ($pCO_{2,t}$, Eq. 3) to calculate the relative influence of non-
 237 thermal and thermal effects on pCO_2 (T/B, Eq. 4). When calculating annual T/B values
 238 with discrete data, only complete years (sampling from January to December) were
 239 included (2014 and 2020 were omitted). When calculating daily T/B values with
 240 continuous data, only complete days (24 hourly measurements) were included.

$$241 \quad pCO_{2,nt} = pCO_{2,obs} \times \exp[\delta \times (T_{mean} - T_{obs})] \quad (2)$$

$$242 \quad pCO_{2,t} = pCO_{2,mean} \times \exp[\delta \times (T_{obs} - T_{mean})] \quad (3)$$

243 where the value for δ ($0.0411 \text{ } ^\circ\text{C}^{-1}$), which represents average $[\partial \ln pCO_2 / \partial$
 244 Temperature] from field observations, was taken directly from Yao and Hu (2017), T_{obs} is
 245 the observed temperature, and T_{mean} is the mean temperature over the investigated time
 246 period.

$$247 \quad T/B = \frac{\max(pCO_{2,thermal}) - \min(pCO_{2,thermal})}{\max(pCO_{2,non-thermal}) - \min(pCO_{2,non-thermal})} \quad (4)$$

248 Where a T/B greater than one indicates that temperature's control on pCO_2 is greater than
 249 the control from non-thermal factors and a T/B less than one indicates that non-thermal
 250 factors' control on pCO_2 is greater than the control from temperature.

251 Tidal control on parameters was investigated using our continuous monitoring
 252 data and tide level data obtained from NOAA's Aransas Pass Station (the Aransas Pass
 253 Station used for windspeed data, < 2 km offshore from monitoring location, Fig. 1) at
 254 [https://tidesandcurrents.noaa.gov/waterlevels.html?id=8775241&name=Aransas,%20Ara](https://tidesandcurrents.noaa.gov/waterlevels.html?id=8775241&name=Aransas,%20Aransas%20Pass&state=TX)
 255 [nsas%20Pass&state=TX](https://tidesandcurrents.noaa.gov/waterlevels.html?id=8775241&name=Aransas,%20Aransas%20Pass&state=TX). Hourly measurements of water level were merged with our
 256 sensor data by date and hour. Given that there were gaps in available water level
 257 measurements (and no measurements prior to December 20, 2016), the usable dataset was

258 reduced from 6088 observations to 5121 observations and fall was omitted from analyses.
259 To examine differences between parameters during high tide and low tide, we defined
260 high tide as tide level greater than the third quartile tide level value and low tide as a tide
261 level less than the first quartile tide level value.

262 Other factors that may exert control on the carbonate system were investigated
263 through parameter relationships. In addition to previously discussed tide and windspeed
264 data, we obtained dissolved oxygen (DO), PAR, turbidity, and chlorophyll fluorescence
265 data from MANERR-deployed environmental sensors that were co-located at our
266 monitoring location (obtained from <https://missionaransas.org/science/download-data>).
267 Given that MANERR data are all measured in the bottom water (>5 m) while our sensors
268 were measuring surface waters, we excluded the observations with significant water
269 column stratification (defined as a salinity difference > 3 between surface water and
270 bottom water) from analyses. Omitting stratified water reduced our continuous dataset
271 from 6088 to 5524 observations (removing 260 winter, 133 spring, 51 summer, and 120
272 fall observations), and omitting observations where there were no MANERR data to
273 determine stratification further reduced the dataset to 4112 observations. Similarly,
274 removing instances of stratification reduced discrete sample data from 104 to 89 surface
275 water observations.

276 *2.6 Statistical Analyses*

277 All statistical analyses were performed in R, version 4.0.3 (R Core Team, 2020).
278 To investigate differences between daytime and nighttime parameter values (temperature,
279 salinity, pH, $p\text{CO}_2$, and CO_2 flux) using continuous monitoring data across the full
280 sampling period and within each season, paired t -tests were used, pairing each respective

281 day's daytime and nighttime values (Table S3). We also used loess models (locally
282 weighted polynomial regression) to identify changes in diel patterns over the course of
283 our monitoring period.

284 Two-way ANOVAs were used to examine differences in parameter means
285 between seasons and between monitoring methods (Table S2). Since there were
286 significant interactions (between season and sampling type factors) in the two-way
287 ANOVAs for each individual parameter (Table S2), differences between seasons were
288 investigated within each monitoring method (one-way ANOVAs) and the differences
289 between monitoring methods were investigated within each season (one-way ANOVAs).
290 For the comparison of monitoring methods, we included both the full discrete sampling
291 data as well as a subset of the discrete sampling data to overlap with the continuous
292 monitoring period (referred to throughout as reduced discrete data or D_C) along with the
293 continuous data. To interpret differences between monitoring methods, a difference in
294 means between the continuous monitoring and discrete monitoring datasets would only
295 indicate that the 10-month period of continuous monitoring was not representative of the
296 5+ year period that discrete samples have been collected, but a difference in means
297 between the continuous data and discrete sample data collected during the continuous
298 monitoring period represents discrepancies between types of monitoring. Post-hoc
299 multiple comparisons (between seasons within sampling types and between sampling
300 types within seasons) were conducted using the Westfall adjustment (Westfall, 1997).

301 Differences in parameters between high tide and low tide conditions were
302 investigated using a two-way ANOVA to model parameters based on tide level and
303 season. In models for each parameter, there was a significant interaction between tide

304 level and season factors (based on $\alpha=0.05$, results not shown), thus t-tests were used
305 (within each season) to examine differences in parameters between high and low tide
306 conditions. Note that fall was omitted from this analysis because tide data were only
307 available at the location beginning December 20, 2016. Sample sizes were the same for
308 each parameter (High tide – winter: 354, spring: 569, summer: 350; Low tide – winter:
309 543, spring: 318, summer: 415).

310 Additionally, to gain insight to carbonate system controls through correlations, we
311 conducted Pearson correlation analyses to examine individual correlations of pH and
312 $p\text{CO}_2$ (both continuous and discrete) with other environmental parameters (Table S5).

313 To better understand overall system variability over different time scales, we used
314 a linear discriminant analysis (LDA), a multivariate statistic that allows dimensional
315 reduction, to determine the linear combination of environmental parameters (individual
316 parameters reduced into linear discriminants, LDs) that allow the best differentiation
317 between day and night as well as between seasons. We included $p\text{CO}_2$, pH, temperature,
318 salinity, tide level, wind speed, total PAR, DO, turbidity, and fluorescent chlorophyll in
319 this analysis. All variables were centered and scaled to allow direct comparison of their
320 contribution to the system variability. The magnitude (absolute value) of coefficients of
321 the LDs (Table 1) represents the relative importance of each individual environmental
322 parameter in the best discrimination between day and night and between seasons, i.e., the
323 greater the absolute value of the coefficient, the more information the associated
324 parameter can provide about whether the sample came from day or night (or winter,
325 spring, or summer). Only one LD could be created for the diel variability (since there are
326 only two classes to discriminate between – day and night). Two LDs could be created for

327 the seasonal variability (since there were three classes to discriminate between – fall was
328 omitted because of the lack of tidal data), but we chose to only report the coefficients for
329 LD1 given that LD1 captured 95.64% of the seasonal variability.

330

331 **3. Results**

332 *3.1 Seasonal variability*

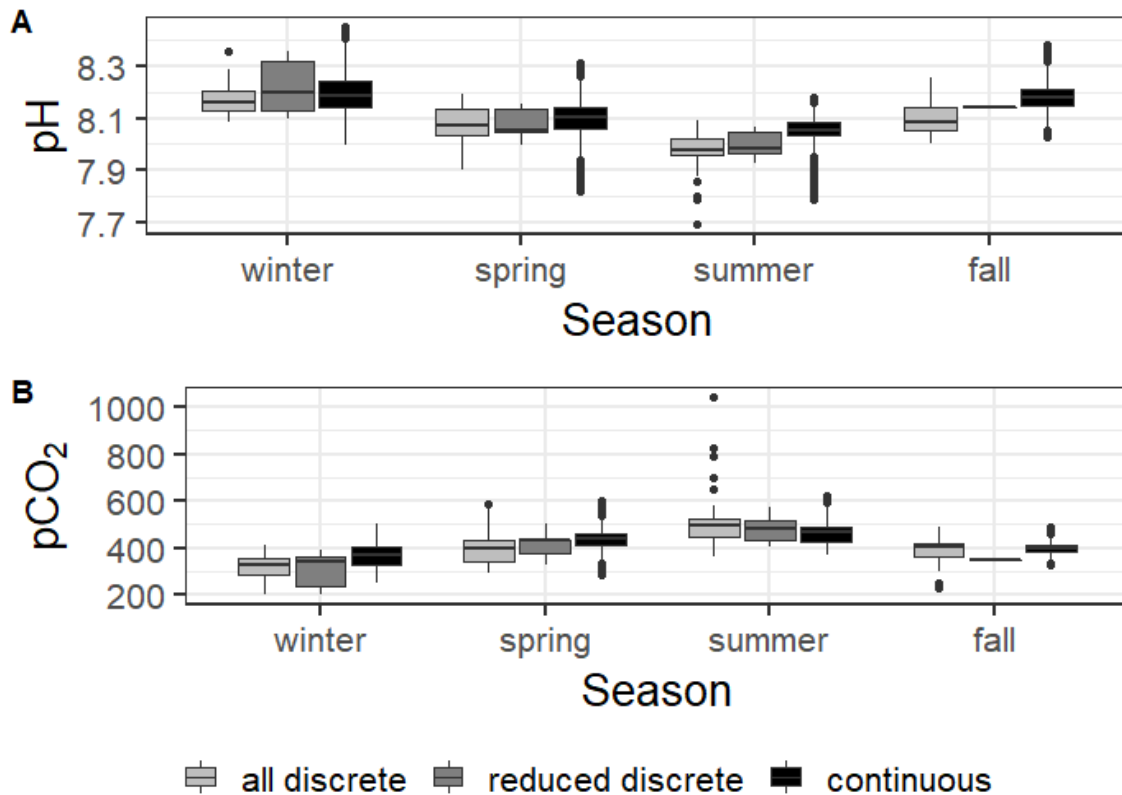
333 Both the continuous and discrete data showed substantial seasonal variability for
334 all parameters (Fig. 2, Tables S1 and S2). All discrete sample results reported here are for
335 the entire 5+ years of monitoring; the subset of discrete sample data that overlaps with
336 the continuous monitoring period will be addressed only in the discussion for method
337 comparisons (Section 4.1.1). Both continuous and discrete data demonstrate significant
338 differences in temperature between each season, with the highest temperature in summer
339 and the lowest in winter (Tables S1 and S2). Mean salinity during sampling periods was
340 highest in the summer and lowest in the fall (Table S1). Significant differences in
341 seasonal salinity occurred between all seasons except spring and winter for continuous
342 data, but only summer differed from other seasons based on discrete data (Tables S1 and
343 S2).

344 Carbonate system parameters also varied seasonally (Fig. 2). For both continuous
345 and discrete data, winter had the highest seasonal pH (8.19 ± 0.08 and 8.162 ± 0.065 ,
346 respectively) and lowest seasonal $p\text{CO}_2$ ($365 \pm 44 \mu\text{atm}$ and $331 \pm 39 \mu\text{atm}$,
347 respectively), while summer had the lowest seasonal pH (8.05 ± 0.06 and 7.975 ± 0.046 ,
348 respectively) and highest seasonal $p\text{CO}_2$ ($463 \pm 48 \mu\text{atm}$ and 511 ± 108 , respectively)

349 (Fig. 2, Table S1). All seasonal differences in pH and $p\text{CO}_2$ were significant, except for
350 the discrete data spring versus fall for both parameters (Table S2).

351

352



353

354

355

356

357

Figure 2. Boxplots of seasonal variability in pH and $p\text{CO}_2$ using all discrete data, reduced discrete data (to overlap with continuous monitoring, Nov. 8 2016 – Aug 23, 2017), and continuous sensor data.

358

359

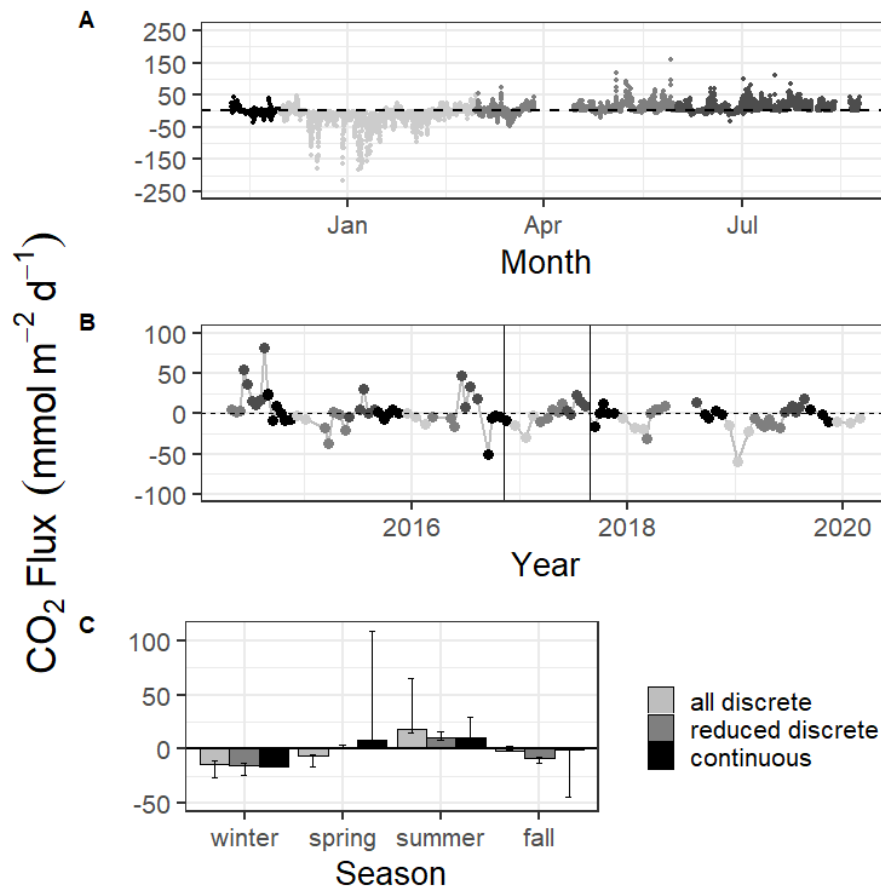
360

361

362

363

Mean CO_2 flux differed by season (Fig. 3, Tables S1 and S2). Both continuous and discrete data records resulted in net negative CO_2 fluxes during fall and winter months, with winter being most negative. Both methods reported a net positive flux for summer, while spring fluxes were positive according to continuous data and negative according to the 5+ years of discrete data (Fig. 3, Table S1). Annual net CO_2 fluxes were near zero (Table S1).



365
 366 **Figure 3.** CO₂ flux calculated over the sampling periods from continuous (A) and
 367 discrete (B) data. Gray scale in (A) and (B) denote different seasons. Vertical lines in (B)
 368 denote the time period of continuous monitoring. (C) shows the seasonal mean CO₂ flux.
 369 Error bars represent mean CO₂ flux using Ho (2006) and Raymond and Cole (2001)
 370 windspeed parameterizations.
 371

372 Results of the LDA incorporated carbonate system parameters along with
 373 additional environmental parameters to get a full picture of system variability over
 374 seasonal timescales (Table 1). The most important parameter in system variability that
 375 allowed differentiation between seasons was temperature (Table 1, Seasonal LD1), as
 376 would be expected with the clear seasonal temperature fluctuations (Fig. S1E). The
 377 second most important parameter for seasonal differentiation was chlorophyll, likely
 378 indicating clear seasonal phytoplankton blooms. The carbonate chemistry also played a

379 critical role in seasonal differentiation, as $p\text{CO}_2$ was the third most important factor
 380 (Table 1).

381 **Table 1.** Coefficients of linear discriminants (LD) from LDA using continuous sensor
 382 data and other environmental parameters. Discriminants for both diel and seasonal
 383 variability shown.

	Seasonal	Diel
	LD1	LD1
Temperature (°C)	-3.53	0.54
Salinity	0.04	0.15
$p\text{CO}_2$ (μatm)	-0.29	-0.16
pH	0.10	0.06
Tide Level (m)	-0.24	0.10
Wind speed (ms^{-1})	0.05	-0.00
Total PAR	-0.07	-2.29
DO (mg L^{-1})	0.09	-0.08
Turbidity	0.15	-0.06
Fluor. Chlorophyll	-0.40	0.14

384

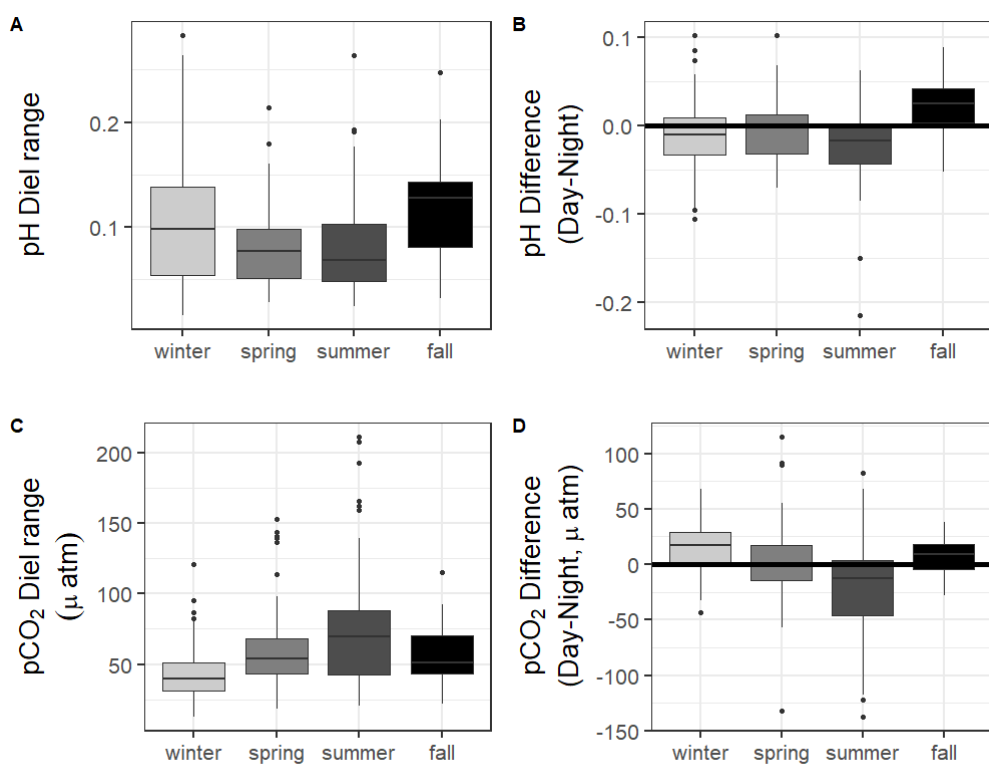
385 *3.2 Diel variability*

386 The 10 months of in-situ continuous monitoring revealed that there was
 387 substantial diel variability in measured parameters (Fig. 4, Table S3). Temperature had a
 388 mean diel range of $1.3 \pm 0.8^\circ\text{C}$ (Table S3). Daytime and nighttime temperature differed
 389 significantly during the summer and fall months, with higher temperatures at night for
 390 both seasons (Table S3). The mean diel range of salinity was 3.4 ± 2.7 (Table S3).
 391 Daytime and nighttime salinity differed significantly during the winter and fall months,
 392 with higher salinities at night for both seasons. The mean diel range of pH was $0.09 \pm$
 393 0.05 (Table S3). Daytime and nighttime pH differed significantly during the winter,
 394 summer, and fall, with nighttime pH significantly higher during summer and winter and
 395 lower during fall (Fig. 4, Table S3). The mean diel range of $p\text{CO}_2$ was $58 \pm 33 \mu\text{atm}$ (Fig.
 396 4, Table S3). Daytime and nighttime $p\text{CO}_2$ differed significantly during the winter and
 397 summer months, with nighttime $p\text{CO}_2$ significantly higher during the summer and lower
 398 during the winter (Fig. 4, Table S3). No significant difference in daytime and nighttime

399 DO were observed during any season (Fig. 5F; paired t-tests, winter $p = 0.1573$, spring p
400 $= 0.4877$, summer $p = 0.794$).

401 Loess models that investigated the evolution of day-night difference in parameters
402 revealed that other environmental parameters, including salinity, temperature, and tide
403 level, also had diel patterns that varied over the duration of our continuous monitoring
404 (Fig. 5).

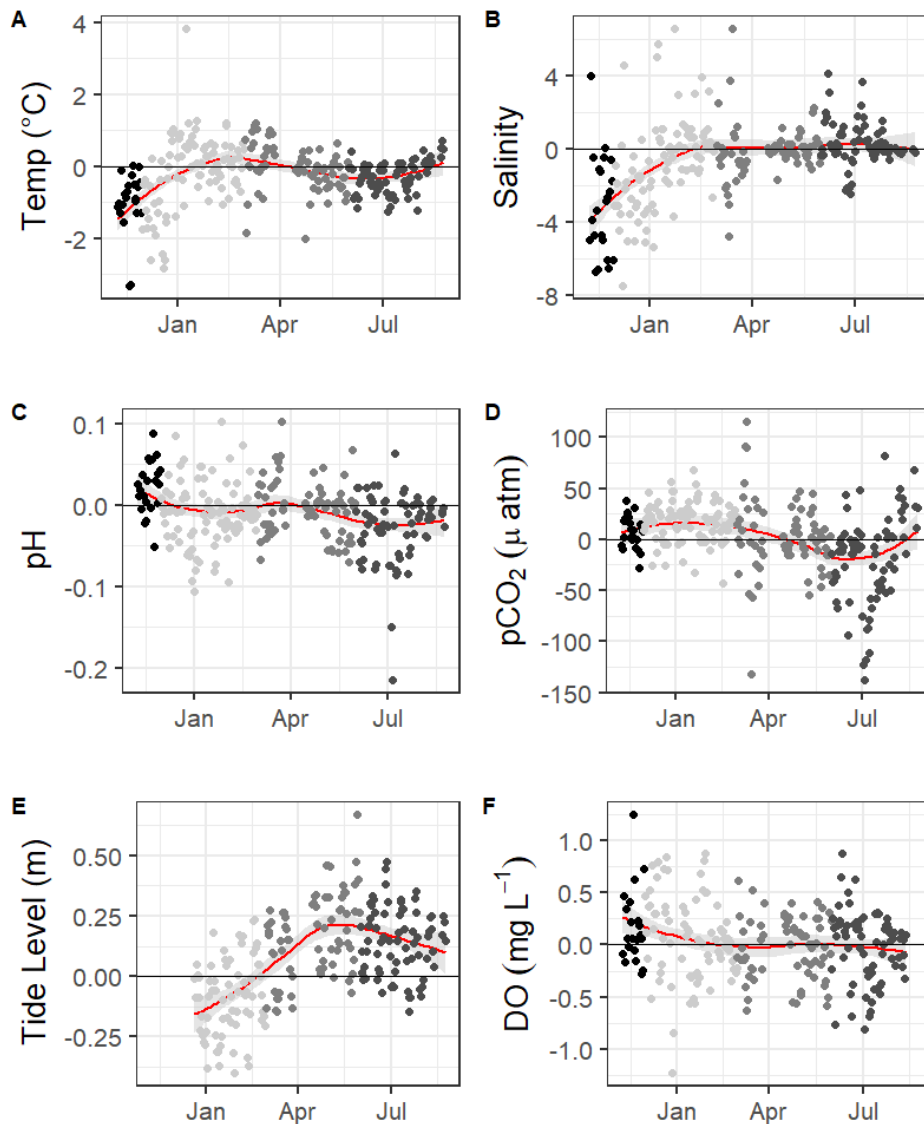
405



406
407 **Figure 4.** Boxplots of the diel range (maximum minus minimum) and difference in daily
408 parameter mean daytime minus nighttime measurements for pH and $p\text{CO}_2$ from
409 continuous sensor data.

410
411 CO_2 flux also fluctuated on a daily scale, with a mean diel range of 34.1 ± 29.0
412 $\text{mmol m}^{-2} \text{d}^{-1}$ (Table S3). However, there was not a significant difference in CO_2 flux of
413 daytime versus nighttime hours for the entire monitoring period or any individual season
414 based on $\alpha=0.05$ (paired t-test, Table S3).

415
416



417
418 **Figure 5.** Loess models (red line) and their confidence intervals (gray bands) showing the
419 difference in daily daytime mean minus nighttime mean measurements. The gray scale of
420 the data points represents the four seasons over which data were collected. Data span
421 from Nov 8, 2016 to Aug 3, 2017, except for the tide data, which began December 20,
422 2016.
423

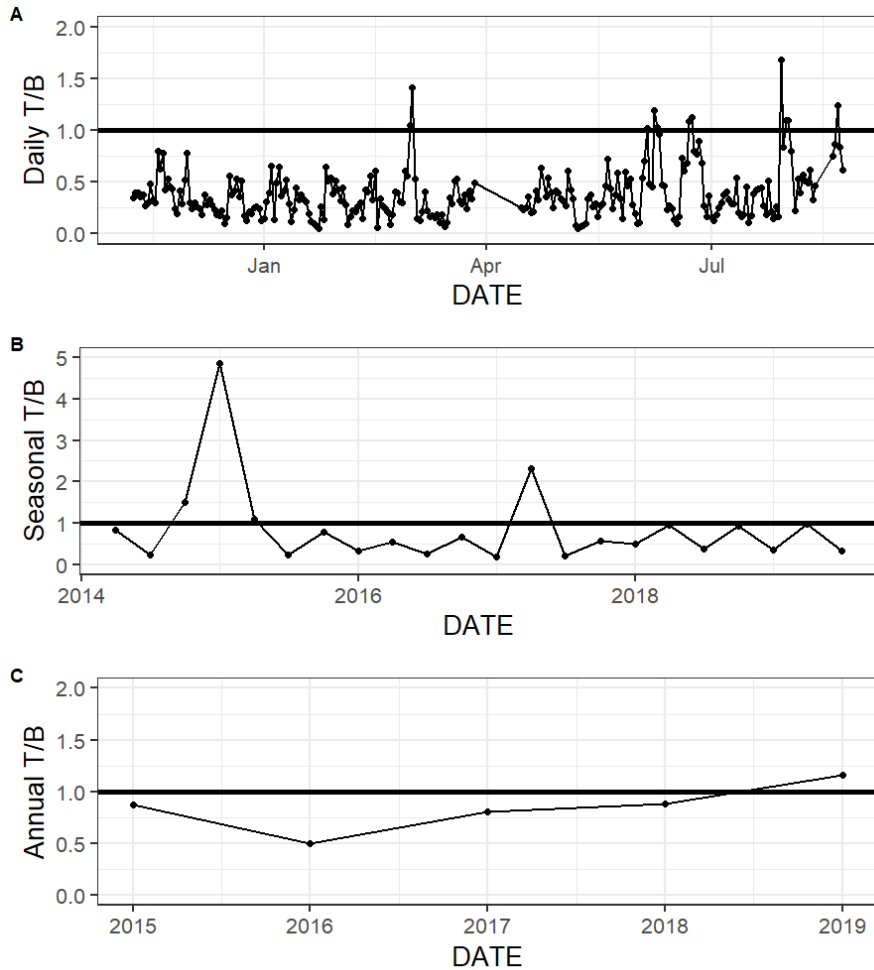
424 Results of the LDA for differentiation between daytime and nighttime conditions
425 revealed that the most important factor was PAR, as would be expected (Table 1, Diel
426 LD1). Temperature was the second most important factor to differentiate between day

427 and night. The carbonate chemistry also played a critical role in day/night differentiation,
428 as $p\text{CO}_2$ was the third most important parameter, providing more evidence for
429 differentiation between day and night than other parameters that would be expected to
430 vary on a diel timescale (e.g., chlorophyll and DO) (Table 1).

431 *3.3 Controlling factors and correlates*

432 The relative influence of thermal and non-thermal factors (T/B) in controlling
433 $p\text{CO}_2$ varied over different time scales (Fig. 6, Table S4). Based on continuous data, non-
434 thermal processes generally exerted more control than thermal processes (T/B<1) over
435 the entire 5+ years of discrete monitoring, within each season, and over most (167/178)
436 days (Fig. 6, Table S4). Annual T/B from discrete data ranged from 0.50 to 1.16, with
437 only one of the five sampled years having T/B greater than one (i.e., more thermal
438 influence; Table S4). While most individual seasons that were sampled experienced
439 stronger non-thermal control on $p\text{CO}_2$ (T/B <1), the only season that never experienced
440 stronger thermal control was summer, with summer T/B values ranging from 0.21 – 0.35
441 for the 6 sampled years (Table S4).

442



443

444 **Figure 6.** Thermal versus non-thermal control on $p\text{CO}_2$ daily (A), seasonal (B), and
 445 annual (C) time scales using both continuous sensor data (daily, from Nov 8, 2016 to Aug
 446 3, 2017) and discrete sample data (seasonal and annual, from May 2, 2014- Feb. 25, 2020).
 447

448 Tidal fluctuations seemed to have a significant effect on carbonate system
 449 parameters (Table 2). Both temperature and salinity were higher at low tide during the
 450 winter and summer months and higher at high tide during the spring. $p\text{CO}_2$ was higher
 451 during low tide during all seasons. pH was higher during high tide during the winter and
 452 summer, but this reversed during the spring, when pH was higher at low tide. CO_2 flux
 453 also varied with tidal fluctuations. CO_2 flux was higher (more positive or less negative) in
 454 the low tide condition for all seasons (though the difference was not significant in

455 spring), i.e., the location was less of a CO₂ sink during low tide conditions in the winter
 456 and more of a CO₂ source during low tide conditions in the summer.

457

458 **Table 2.** Mean and standard deviation of temperature, salinity, pH, *p*CO₂, and calculated
 459 CO₂ flux (from continuous sensor measurements) during high and low tide conditions.

460

Parameter	Season	High Tide Mean	Low Tide Mean	Difference between tide levels, t-test p-value
Temperature (°C)	Winter	16.7 ± 1.7	17.6 ± 2.0	<0.0001
	Spring	24.4 ± 2.7	23.6 ± 2.7	<0.0001
	Summer	29.3 ± 0.5	30.1 ± 0.7	<0.0001
Salinity	Winter	30.2 ± 2.5	31.3 ± 2.9	<0.0001
	Spring	30.4 ± 1.9	30.0 ± 2.7	0.0071
	Summer	30.5 ± 2.4	34.5 ± 3.0	<0.0001
pH	Winter	8.20 ± 0.08	8.15 ± 0.06	<0.0001
	Spring	8.07 ± 0.09	8.10 ± 0.07	<0.0001
	Summer	8.08 ± 0.04	8.04 ± 0.06	<0.0001
<i>p</i>CO₂ (µatm)	Winter	331 ± 40	378 ± 42	<0.0001
	Spring	435 ± 33	443 ± 50	0.0154
	Summer	419 ± 30	482 ± 48	<0.0001
CO₂ Flux (mmol m⁻² d⁻¹)	Winter	-33.0 ± 38.1	-11.7 ± 21.8	<0.0001
	Spring	7.4 ± 14.0	8.7 ± 14.8	0.2248
	Summer	1.8 ± 6.3	16.0 ± 14.5	<0.0001

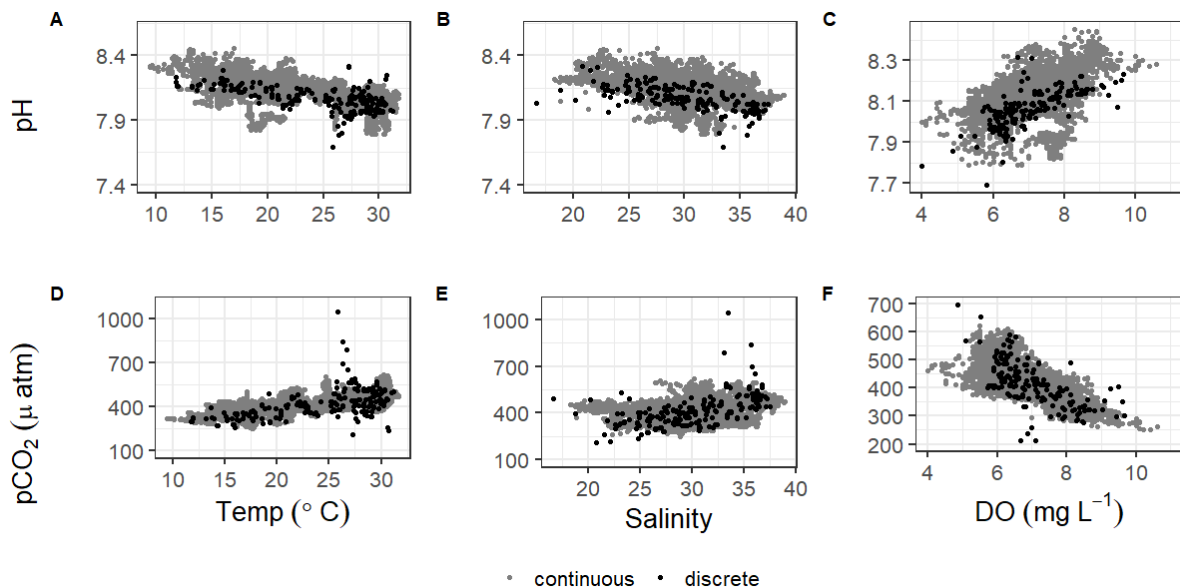
461

462 Mean water level varied between all seasons; mean spring (highest) water levels
 463 were on average 0.08 m higher than winter (lowest) water levels (ANOVA *p*<0.0001, fall
 464 was not considered because of a lack of water level data). The mean daily tidal range
 465 during our continuous monitoring period was 0.39 m ± 0.13 m, which did not
 466 significantly differ between seasons (ANOVA *p*=0.739). However, the day-night
 467 difference in tide level exhibited a strong seasonality, with spring and summer having
 468 higher tide level during the daytime and winter having higher tide level during the
 469 nighttime (Fig. 5).

470 There were significant correlations between carbonate system parameters (pH and
 471 *p*CO₂) and many of the other environmental parameters, including windspeed, DO,

472 turbidity, and fluorescent chlorophyll (Figure 7, Table S5). Both the continuous and
473 discrete sampling types indicate that pH has a significant negative relationship with both
474 temperature and salinity and $p\text{CO}_2$ has a significant positive relationship with both
475 temperature and salinity (Fig. 7). However, correlations with temperature were stronger
476 for continuous data and correlations with salinity were stronger for discrete data (Table
477 S5). The strongest correlations between continuous carbonate system data and all
478 investigated environmental parameters were with DO (positive correlation with pH and
479 negative correlation with $p\text{CO}_2$; Table S5). It is worth noting that there were no
480 observations of hypoxia at our study site during our monitoring, with minimum DO
481 levels of 3.9 mg L^{-1} and 4.0 mg L^{-1} for our continuous monitoring period and our discrete
482 sampling period, respectively.

483
484



485
486 **Figure 7.** Correlations of pH and $p\text{CO}_2$ with temperature, salinity, and DO from
487 continuous sensor data (gray) and all discrete data (black).
488

489 **Discussion**

490 *4.1 Comparing continuous monitoring and discrete sampling: Representative sampling in*
491 *a temporally variable environment*

492 Discrete water sample collection and analysis is the most common method that
493 has been employed to attempt to understand the carbonate system of estuaries. However,
494 it is difficult to know if these samples are representative of the spatial and temporal
495 variability in carbonate system parameters. While this time-series study cannot conclude
496 whether our broader sampling efforts in the MAE are representative of the spatial
497 variability in the estuary, it can investigate how representative our bimonthly to monthly
498 sampling is of the more high-frequency temporal variability that ASC experiences.

499 There were several instances where seasonal parameter means significantly
500 differed between the 10-month continuous monitoring period and the 5+ year discrete
501 sampling period (Table S2, $C \neq D$ or $D_c \neq D$) including temperature in the summer and
502 fall, salinity in the spring, pH in the summer and fall, and $p\text{CO}_2$ in winter, spring, and
503 summer. While clear seasonal variability was demonstrated for most parameters (using
504 both continuous and discrete data for the entire period), these differences between the 10-
505 month continuous monitoring period and our 5+ year monitoring period illustrate that
506 there is also interannual variability in the system. Therefore, short periods of monitoring
507 are unable to fully capture current baseline conditions.

508 During the continuous monitoring period (2016-2017), we found no significant
509 difference between sampling methods in the seasonal mean temperature, salinity, or
510 $p\text{CO}_2$. The two sampling methods also resulted in the same mean pH for all seasons
511 except for summer, when the sensor data recorded a higher mean pH than discrete

512 samples (Tables S1 and S2). During this case, we can conclude that discrete monitoring
513 did not accurately represent the system variability that was able to be captured by the
514 sensor monitoring. However, given that most seasons did not show differences in pH or
515 $p\text{CO}_2$ between sampling methods, the descriptive statistics associated with the discrete
516 monitoring did a fair job of representing system means. This is evidence that long-term
517 discrete monitoring efforts, which are much more widespread in estuarine systems than
518 sensor deployments, can be generally representative of the system despite known
519 temporal variability on shorter time scales. However, further study would be needed to
520 determine if this applies throughout the system, as the upper estuary generally
521 experiences greater variability.

522 Understanding the relationships of pH and $p\text{CO}_2$ with temperature and salinity is
523 important in a system (Fig. 7). Based on the results of an Analysis of Covariance
524 (ANCOVA), the relationship (slope) of pH with both temperature and salinity and of
525 $p\text{CO}_2$ with salinity were not significantly different between types of monitoring
526 (considering the sensor deployment period only), supporting the effectiveness of long-
527 term discrete monitoring programs when sensors are unable to be deployed. However,
528 ANCOVA did reveal the relationship of $p\text{CO}_2$ with temperature is significantly different
529 (method:temp $p=0.0062$) between monitoring methods.

530 The high temporal resolution of sensor data is presumably better for estimating
531 CO_2 flux at a given location than discrete sampling. Previous studies have pointed out
532 that discrete sampling methods, which generally involve only daytime sampling, do not
533 adequately capture the diel variability in the carbonate system and may therefore lead to
534 biased CO_2 fluxes (Crosswell et al., 2017; Liu et al., 2016). However, we found no

535 significant difference (within any season) between CO₂ flux values calculated with
536 hourly sensor data versus single, discrete samples collected monthly to twice monthly
537 (Table S2, Fig. 3). Calculated CO₂ fluxes also did not significantly differ between day
538 and night during any season, despite some differences in *p*CO₂ (Table S3), likely due to
539 the large error associated with the calculation of CO₂ flux (Table S1, Fig. 3) which will
540 be further discussed below. Therefore, the expected underestimation of CO₂ flux based
541 on diel variability of *p*CO₂ was not encountered at our study site, validating the use of
542 discrete samples for quantification of CO₂ fluxes (until methods with less associated error
543 are available). Even given less error in calculated flux, estimated fluxes would likely not
544 differ between methods on an annual scale (as *p*CO₂ did not), but CO₂ fluxes may differ
545 on a seasonal scale since the differences between daytime and nighttime *p*CO₂ were not
546 consistent across seasons (Table S3, Fig. 4).

547 There are many factors contributing to error associated with CO₂ flux. There is
548 still large error associated with estimates of estuarine CO₂ flux because turbulent mixing
549 is difficult to model and turbulence is the main control on CO₂ gas transfer velocity, *k*, in
550 shallow water environments. Thus, our wind speed parameterization of *k* is imperfect and
551 likely the greatest source of error (Borges and Abril, 2011; Van Dam et al., 2019). Other
552 notable sources of error include the data treatment. For example, we chose to seasonally
553 weight the individual calculated flux values in the calculation of annual flux to account
554 for differences in sampling frequency between seasons. From continuous data, the
555 weighted average flux was 0.2 mmol m⁻² d⁻¹, although choosing not to seasonally weight
556 and simply look at the arithmetic mean of fluxes calculated directly from sampling dates
557 would have resulted in an annual CO₂ flux of -0.7 mmol m⁻² d⁻¹ for the same period.

558 Similarly, the weighted average flux from all 5+ years of discrete data was -0.9 mmol m^{-2}
559 d^{-1} , but the arithmetic mean of fluxes would have resulted in an annual CO_2 flux of 0.2
560 $\text{mmol m}^{-2} \text{ d}^{-1}$ for the same period. Another source of error that could be associated with
561 the calculation of flux from the discrete data is the way in which wind speed data are
562 aggregated to be used in the windspeed parameterization. We decided to use daily
563 averages of the windspeed for calculations. Using the windspeed measured for the closest
564 time to our sampling time or the monthly averaged wind speed may have resulted in very
565 different flux values.

566

567 *4.2 Factors controlling temporal variability in carbonate system parameters*

568 Our study site had a relatively small range of pH and $p\text{CO}_2$ on both diel and
569 seasonal scales compared to other coastal regions (Challener et al., 2016; Yates et al.,
570 2007). This small variability is likely tied to a combination of the subtropical setting
571 (small temperature variability), the lower estuary position of our monitoring (further
572 removed from the already small freshwater influence), little ocean upwelling influence,
573 and the system's relatively high buffer capacity that results from the high alkalinity of the
574 freshwater endmembers (Yao et al., 2020). Just as the extent of hypoxia-induced
575 acidification was relatively low in Corpus Christi Bay because of the bay's high buffer
576 capacity (McCutcheon et al., 2019), the extent of pH fluctuation resulting from all
577 controlling factors at ASC would also be modulated by the region's high intrinsic buffer
578 capacity.

579 *4.2.1 Thermal and biological controls on carbonate chemistry*

580 We demonstrated that both temperature and non-thermal processes exert control
581 on $p\text{CO}_2$, but non-thermal control generally surpasses thermal control in ASC over

582 multiple time scales (Fig. 6, Table S4, $T/B < 1$). The magnitude of $p\text{CO}_2$ variation
583 attributed to non-thermal processes varied greatly (i.e., $\Delta p\text{CO}_{2,\text{nt}}$ had large standard
584 deviations, Table S4). For example, during the year of strongest non-thermal control
585 (2016), $\Delta p\text{CO}_{2,\text{nt}}$ was 534 μatm versus $\Delta p\text{CO}_{2,\text{nt}}$ of 209 μatm in the year of weakest
586 thermal control (2019). Conversely, the magnitude of $p\text{CO}_2$ variation attributed to
587 temperature was consistent across time scales. For example, during the year of strongest
588 thermal control (2015), $\Delta p\text{CO}_{2,\text{t}}$ was 276 μatm versus $\Delta p\text{CO}_{2,\text{t}}$ of 242 μatm in the year of
589 weakest thermal control (2017). Spring and fall seasons, which experienced the greatest
590 temperature swings (Table S1), had greater relative temperature control exerted on $p\text{CO}_2$
591 out of all seasons (Fig. 6, Table S4). The difference in T/B between sampling methods is
592 relatively small over the 10-month sensor deployment period, but it is worth noting that
593 T/B did not align over shorter seasonal time scales sampling methods (Fig. 6, Table S4).
594 Continuous monitoring demonstrated a greater magnitude of fluctuation resulting from
595 both temperature and non-thermal processes (i.e., greater $\Delta p\text{CO}_{2,\text{t}}$ and $\Delta p\text{CO}_{2,\text{nt}}$),
596 indicating that the extremes are generally not captured by the discrete, daytime sampling,
597 and sensor data would provide a better understanding of system controls.

598 The greater influence of non-thermal controls that we report conflicts with Yao
599 and Hu (2017), who found that ASC was primarily thermally controlled (T/B 1.53 – 1.79)
600 from May 2014 to April 2015. Yao and Hu (2017) also found that locations in the upper
601 estuary experienced lower T/B during flooding conditions than drought conditions.
602 Although the opposite was found at ASC, it is likely that the high T/B calculated at ASC
603 by Yao and Hu (2017) was still a result of the drought condition due to the long residence
604 time of the estuary. Since 2015, there has not been another significant drought in the

605 system, so it seems that non-thermal controls on $p\text{CO}_2$ are more important at this location
606 under normal freshwater inflow conditions.

607 Significantly warmer water temperatures were observed during the nighttime in
608 both summer and fall (Fig. 5), indicating that temperature could exert a slight control on
609 the carbonate system over a diel time scale. We note that significant differences in day
610 and night temperature within seasons do not indicate that diel differences were observed
611 on all days within the season, as large standard deviations in both daytime and nighttime
612 values result in considerable overlap. More substantial temperature swings between
613 seasons would result in more temperature control over a seasonal timescale. ASC seems
614 to have less thermal control of the carbonate system than offshore GOM waters, as
615 temperature had substantially higher explanatory value for pH and $p\text{CO}_2$ based on simple
616 linear regressions in offshore GOM waters ($R^2 = 0.81$ and 0.78 , respectively (Hu et al.,
617 2018)) than at ASC ($R^2 = 0.30$ and 0.52 , respectively, for sensor data and $R^2 = 0.38$ and
618 0.25 , respectively, for discrete data).

619 Though annual average $p\text{CO}_2$ (and CO_2 flux) are higher in the upper MAE and
620 lower offshore than at our study site, the same seasonal patterns that we observed (i.e.,
621 elevated $p\text{CO}_2$ and positive CO_2 flux in the summer and depressed $p\text{CO}_2$ and negative
622 CO_2 flux during the winter, Table S1, Fig. S1) has also been observed throughout the
623 entire MAE and the open Gulf of Mexico (Hu et al., 2018; Yao and Hu, 2017). These
624 seasonal patterns correspond with both the directional response of the system to
625 temperature and net community metabolism response to changing temperature, i.e.,
626 elevated respiration in summer months (Caffrey, 2004). Despite that there were no
627 observations of hypoxia, there was a strong relationship between the carbonate system

628 parameters and DO (Fig. 7, Table S5), suggesting that net ecosystem metabolism may
629 exert an important control on the carbonate system on seasonal time scales. The lack of
630 day-night difference in DO (Fig. 5F) despite the significant day-night difference in both
631 pH and $p\text{CO}_2$ suggests that net community metabolism is likely not a strong controlling
632 factor on diel time scales. Biological control likely becomes more important over
633 seasonal timescales.

634 *4.2.2 Tidal control on carbonate chemistry*

635 While the tidal range in the northwestern GOM is relatively small (1.30 m over
636 our 10-month continuous monitoring period), the tidal inlet location of our study site
637 results in proportionally more “coastal water” during high tide and proportionally more
638 “estuarine water” during low tide. The carbonate chemistry signal of these different water
639 masses was seen in the differences between high tide and low tide conditions at ASC
640 (i.e., high tide having lower $p\text{CO}_2$ because coastal waters are less heterotrophic than
641 estuarine waters, Table 2). Consequently, the relative importance of thermal versus non-
642 thermal controls may be modulated by tide level. We calculated the thermal and non-
643 thermal $p\text{CO}_2$ terms separately during high tide and low tide periods and found that non-
644 thermal control is more important during low tide conditions (within each season T/B is
645 0.10 ± 0.07 lower during the low tide than high tide). This is likely because low tide has
646 proportionally more “estuarine water” at the location and because there is less volume of
647 water for the end products of biological processes to accumulate. The difference in T/B
648 between high tide and low tide conditions was greatest in the spring, likely due to a
649 combination of elevated spring-time productivity and larger tidal ranges in the spring.

650 The GOM is one of the few places in the world that experiences diurnal tides
651 (Seim et al., 1987; Thurman, 1994), so theoretically, the fluctuations in $p\text{CO}_2$ associated
652 with tides may align to either amplify or reduce/reverse the fluctuations that would result
653 from diel variability in net community metabolism. Based on diel tidal fluctuations at this
654 site (i.e., higher tides during the day in the spring and summer and higher tides at night
655 during the winter, Fig. 5E) and the higher $p\text{CO}_2$ associated with low tide (Table 2), tidal
656 control should amplify the biological signal (nighttime $p\text{CO}_2 > \text{daytime } p\text{CO}_2$) during
657 spring and summer and reduce or reverse the biological signal during the winter. This
658 tidal control can explain the diel variability present in our $p\text{CO}_2$ data, which showed the
659 full reversal of the expected biological signal in the winter (Fig. 5C, Table S3, nighttime
660 $p\text{CO}_2 < \text{daytime } p\text{CO}_2$), i.e., the higher nighttime tides in winter brought in enough low
661 CO_2 water from offshore to fully offset any nighttime buildup of CO_2 from the lack of
662 photosynthesis. However, we note that the expected diel, biological control was likely
663 minimal since daytime DO was not consistently higher than nighttime DO (Fig. 5F). The
664 same seasonal pattern diel tide fluctuations were exhibited from Dec 20, 2016 (when the
665 tide data is first available) through the rest of our discrete monitoring period (Feb 25,
666 2020), indicating that tidal control on diel variability of carbonate system parameters was
667 likely consistent throughout this 3+ year period. The diel variability in pH did not mirror
668 $p\text{CO}_2$ as would be expected (Fig. 5). The relationship between pH and tide level more
669 closely mirrored the relationships of salinity and temperature with tide level (versus $p\text{CO}_2$
670 relationship with tide level; Table 2), indicating that controlling factors of the carbonate
671 system may not be exerted equally on both pH and $p\text{CO}_2$ over different time scales.
672 *4.2.3 Salinity and freshwater inflow controls on carbonate chemistry*

673 Previous studies have indicated that freshwater inflow may exert a primary
674 control on the carbonate system in the estuaries of the northwestern GOM (Hu et al.,
675 2015; Yao et al., 2020; Yao and Hu, 2017). Though the river water still has elevated
676 $p\text{CO}_2$ and depressed pH compared to the seawater endmember, the high riverine
677 alkalinity (often higher than the seawater endmember) in the region results in relatively
678 well-buffered estuarine conditions in MAE (Yao and Hu, 2017). Carbonate system
679 variability is much lower at ASC than it is in the more upper reaches of MAE, likely due
680 to the lesser influence of freshwater inflow and its associated changes in biological
681 activity at ASC (Yao and Hu, 2017). Given the location of our sampling in the lower
682 portion of the estuary and the long residence time in the system, we did not directly
683 address river discharge as a controlling factor, but the influence of freshwater inflow may
684 be evident in the response of the system to changes in salinity. Fluctuating salinity at
685 ASC may also result from direct precipitation, stratification, and tidal fluctuations;
686 however, the low R^2 (0.02) associated with a simple linear regression between tide level
687 and salinity ($p < 0.0001$) indicates that salinity fluctuations are more indicative of non-tidal
688 factors. Salinity data from both sensor and discrete monitoring were strongly correlated
689 with both pH and $p\text{CO}_2$, with correlation coefficients nearing (continuous) or surpassing
690 (discrete) that of the correlations with temperature (Fig. 7; Table S5). Periods of lower
691 salinity had higher pH and lower $p\text{CO}_2$, likely due to enhanced freshwater influence and
692 subsequent elevated primary productivity at the study site.

693 *4.2.4 Windspeed and CO_2 inventory*

694 We investigated wind speed as a possible control on the carbonate system to gain
695 insight into the effect of wind-driven CO_2 fluxes on the inventory of CO_2 in the water

696 column (and subsequent impacts to the entire carbonate system). The Texas coast has
697 relatively high wind speeds, with the mean wind speed observed during our continuous
698 monitoring period being 5.8 m s^{-1} . While this results in relatively high calculated CO_2
699 fluxes (Fig. 3), the seasonal relationship between $p\text{CO}_2$ and windspeed does not support a
700 change in inventory with higher winds. Since spring and summer both have a mean
701 estuarine $p\text{CO}_2$ greater than atmospheric level (and positive CO_2 flux, Table S1) a
702 negative relationship between windspeed and $p\text{CO}_2$ would be necessary to support this
703 hypothesis, but winter, spring, and fall all experience increases in $p\text{CO}_2$ with increasing
704 wind based on simple linear regression.

705 *4.3 Carbonate chemistry as a component of overall system variability*

706 Estuaries and coastal areas are dynamic systems with human influence, riverine
707 influence, and influence from an array of biogeochemical processes, resulting in highly
708 variable environmental conditions. Based on an LDA used to assess overall system
709 variability using a suite of environmental parameters compiled at a single location, we
710 can conclude that carbonate chemistry parameters are among the most important of
711 variants on both daily and seasonal time scales in this coastal setting. Of the two
712 carbonate system components that we incorporated (pH and $p\text{CO}_2$), $p\text{CO}_2$ was the most
713 critical in discriminating along diel or seasonal scales despite similar seasonal differences
714 that were identified by ANOVA (Table S2) and more seasons with significant diel
715 differences in pH (Table S3). pH seemed to be a larger component of overall system
716 variability on a seasonal time scale (compared to the very small contribution seen on a
717 diel scale, Table 1). Given that the seasonal and diel variability in carbonate chemistry at
718 this location is relatively small compared to other coastal areas that are in the literature,

719 the high contribution of carbonate chemistry to overall system variability that we detected
720 is likely to be present at other coastal locations around the world.

721 **5. Conclusions**

722 We monitored carbonate chemistry parameters (pH and $p\text{CO}_2$) using both sensor
723 deployments (10 months) and discrete sample collection (5+ years) at the Aransas Ship
724 Channel, TX, to characterize temporal variability. Significant seasonal variability and
725 diel variability in carbonate system parameters were both present at the location. Diel
726 fluctuations were smaller than many other areas previously studied. The difference
727 between daytime and nighttime values of carbonate system parameters varied between
728 seasons, occasionally reversing the expected diel variability due to biological processes.
729 Tide level (despite the small tidal range), temperature, freshwater influence, and
730 biological activity all seem to exert important controls on the carbonate system at the
731 location. The relative importance of the different controls varied with timescale, and
732 controls were not always exerted equally on both pH and $p\text{CO}_2$. Carbonate chemistry
733 (particularly $p\text{CO}_2$) was among the most important environmental parameters to in
734 overall system variability to distinguish between both diel and seasonal environmental
735 conditions.

736 Despite known temporal variability on shorter timescales, discrete sampling was
737 generally representative of the average carbonate system on a seasonal and annual basis
738 based on comparison with our sensor data. Discrete data captured interannual variability,
739 which could not be captured by the shorter-term continuous sensor data. Additionally,
740 there was no difference in CO_2 flux between sampling types. All of these findings

741 support the validity of discrete sample collection for carbonate system characterization at
742 this location.

743 This is one of the first studies that investigates high-temporal frequency data from
744 deployed sensors that measure carbonate system parameters in an estuary-influenced
745 environment. Long-term, effective deployments of these monitoring tools could greatly
746 improve our understanding of estuarine systems. This study's detailed investigation of
747 data from multiple, co-located environmental sensors was able to provide insight into
748 potential driving forces of carbonate chemistry on diel and seasonal time scales; this
749 provides strong support for the implementation of carbonate chemistry monitoring in
750 conjunction with preexisting coastal environmental monitoring infrastructure.

751 Strategically locating such sensors in areas that are subject to local acidification drivers
752 or support large biodiversity or commercially important species may be the most crucial
753 in guiding future mitigation and adaptation strategies for natural systems and aquaculture
754 facilities.

755

756 **Data availability**

757 Continuous sensor data are archived with the National Oceanic and Atmospheric
758 Administration's (NOAA's) National Centers for Environmental Information (NCEI)
759 (<https://doi.org/10.25921/dkg3-1989>). Discrete sample data are available in two separate
760 datasets archived with National Science Foundation's Biological & Chemical
761 Oceanography Data Management Office (BCO-DMO) (doi:10.1575/1912/bco-
762 dmo.784673.1 and doi: 10.26008/1912/bco-dmo.835227.1).

763 **Author Contribution**

764 MM and XH defined the scope of this work. XH received funding for all components of
765 the work. MM, HY, and CJS performed field sampling and laboratory analysis of
766 samples. MM prepared the initial manuscript and all co-authors contributed to revisions.

767 **Competing interests**

768 The authors declare that they have no conflict of interest.

769

770 **Acknowledgements**

771 Funding for autonomous sensors and sensor deployment was provided by the
772 United States Environmental Protection Agency's National Estuary Program via the
773 Coastal Bend Bays and Estuaries Program Contract No. 1605. Thanks to Rae Mooney
774 from Coastal Bend Bays and Estuaries Program for assistance in the initial sensor setup.
775 Funding for discrete sampling as well MM's dissertation research has been supported by
776 both NOAA National Center for Coastal Ocean Science (Contract No.
777 NA15NOS4780185) and NSF Chemical Oceanography Program (OCE-1654232). We
778 also appreciate the support from the Mission-Aransas National Estuarine Research
779 Reserve in allowing us the boat-of-opportunity for our ongoing discrete sample
780 collections and the University of Texas Marine Science Institute for allowing us access to
781 their research pier for the sensor deployment. A special thanks to Hongjie Wang, Lisette
782 Alcocer, Allen Dees, and Karen Alvarado for assistance with field work. We would also
783 like to thank Melissa Ward, our other anonymous referee, and the Associate Editor, Tyler
784 Cyronak, for aiding in the considerable improvement of this manuscript.

785 **References**

- 786 Barton, A., Waldbusser, G.G., Feely, R.A., Weisberg, S.B., Newton, J.A., Hales, B.,
787 Cudd, S., Eudeline, B., Langdon, C.J., Jefferds, I., King, T., Suhrbier, A.,
788 McLaughlin, K., 2015. Impacts of coastal acidification on the pacific northwest
789 shellfish industry and adaptation strategies implemented in response. *Oceanography*
790 28, 146–159.
- 791 Bednaršek, N., Tarling, G.A., Bakker, D.C.E., Fielding, S., Jones, E.M., Venables, H.J.,
792 Ward, P., Kuzirian, A., Lézé, B., Feely, R.A., Murphy, E.J., 2012. Extensive
793 dissolution of live pteropods in the Southern Ocean. *Nat. Geosci.* 5, 881–885.
794 <https://doi.org/10.1038/ngeo1635>
- 795 Borges, A. V., 2005. Do we have enough pieces of the jigsaw to integrate CO₂ fluxes in
796 the coastal ocean ? *Estuaries* 28, 3–27.
- 797 Borges, A. V., Abril, G., 2011. Carbon Dioxide and Methane Dynamics in Estuaries,
798 *Treatise on Estuarine and Coastal Science*. [https://doi.org/10.1016/B978-0-12-](https://doi.org/10.1016/B978-0-12-374711-2.00504-0)
799 [374711-2.00504-0](https://doi.org/10.1016/B978-0-12-374711-2.00504-0)
- 800 Bresnahan, P.J., Martz, T.R., Takeshita, Y., Johnson, K.S., LaShomb, M., 2014. Best
801 practices for autonomous measurement of seawater pH with the Honeywell Durafet.
802 *Methods Oceanogr.* 9, 44–60. <https://doi.org/10.1016/j.mio.2014.08.003>
- 803 Caffrey, J.M., 2004. Factors controlling net ecosystem metabolism in U.S. estuaries.
804 *Estuaries* 27, 90–101. <https://doi.org/10.1007/BF02803563>
- 805 Cai, W.-J., 2011. Estuarine and Coastal Ocean Carbon Paradox: CO₂ Sinks or Sites of
806 Terrestrial Carbon Incineration? *Ann. Rev. Mar. Sci.* 3, 123–145.
807 <https://doi.org/10.1146/annurev-marine-120709-142723>

808 Cai, W.-J., Hu, X., Huang, W.-J., Murrell, M.C., Lehrter, J.C., Lohrenz, S.E., Chou, W.-
809 C., Zhai, W., Hollibaugh, J.T., Wang, Y., Zhao, P., Guo, X., Gundersen, K., Dai, M.,
810 Gong, G.-C., 2011. Acidification of subsurface coastal waters enhanced by
811 eutrophication. *Nat. Geosci.* 4, 766–770. <https://doi.org/10.1038/ngeo1297>

812 Challener, R.C., Robbins, L.L., McClintock, J.B., 2016. Variability of the carbonate
813 chemistry in a shallow, seagrass-dominated ecosystem: Implications for ocean
814 acidification experiments. *Mar. Freshw. Res.* 67, 163–172.
815 <https://doi.org/10.1071/MF14219>

816 Crosswell, J.R., Anderson, I.C., Stanhope, J.W., Van Dam, B., Brush, M.J., Ensign, S.,
817 Piehler, M.F., McKee, B., Bost, M., Paerl, H.W., 2017. Carbon budget of a shallow,
818 lagoonal estuary: Transformations and source-sink dynamics along the river-estuary-
819 ocean continuum. *Limnol. Oceanogr.* 62, S29–S45.
820 <https://doi.org/10.1002/lno.10631>

821 Cyronak, T., Andersson, A.J., D’Angelo, S., Bresnahan, P., Davidson, C., Griffin, A.,
822 Kindeberg, T., Pennise, J., Takeshita, Y., White, M., 2018. Short-term spatial and
823 temporal carbonate chemistry variability in two contrasting seagrass meadows:
824 Implications for pH buffering capacities. *Estuaries and Coasts* 41, 1282–1296.
825 <https://doi.org/10.1007/s12237-017-0356-5>

826 Dickson, A.G., 1990. Standard potential of the reaction: $\text{AgCl(s)} + \frac{1}{2}\text{H}_2(\text{g}) = \text{Ag(s)} +$
827 HCl(aq) , and the standard acidity constant of the ion HSO_4^- in synthetic sea
828 water from 273.15 to 318.15 K. *J. Chem. Thermodyn.* 22, 113–127.
829 [https://doi.org/10.1016/0021-9614\(90\)90074-Z](https://doi.org/10.1016/0021-9614(90)90074-Z)

830 Ekstrom, J. a., Suatoni, L., Cooley, S.R., Pendleton, L.H., Waldbusser, G.G., Cinner, J.E.,

831 Ritter, J., Langdon, C., van Hooideonk, R., Gledhill, D., Wellman, K., Beck, M.W.,
832 Brander, L.M., Rittschof, D., Doherty, C., Edwards, P.E.T., Portela, R., 2015.
833 Vulnerability and adaptation of US shellfisheries to ocean acidification. *Nat. Clim.*
834 *Chang.* 5, 207–214. <https://doi.org/10.1038/nclimate2508>

835 Gazeau, F., Quiblier, C., Jansen, J.M., Gattuso, J.-P., Middelburg, J.J., Heip, C.H.R.,
836 2007. Impact of elevated CO₂ on shellfish calcification. *Geophys. Res. Lett.* 34,
837 L07603. <https://doi.org/10.1029/2006GL028554>

838 Gobler, C.J., Talmage, S.C., 2014. Physiological response and resilience of early life-
839 stage Eastern oysters (*Crassostrea virginica*) to past, present and future ocean
840 acidification. *Conserv. Physiol.* 2, 1–15.
841 <https://doi.org/10.1093/conphys/cou004>.Introduction

842 Ho, D.T., Law, C.S., Smith, M.J., Schlosser, P., Harvey, M., Hill, P., 2006.
843 Measurements of air-sea gas exchange at high wind speeds in the Southern Ocean:
844 Implications for global parameterizations. *Geophys. Res. Lett.* 33, 1–6.
845 <https://doi.org/10.1029/2006GL026817>

846 Hofmann, G.E., Smith, J.E., Johnson, K.S., Send, U., Levin, L. a, Micheli, F., Paytan, A.,
847 Price, N.N., Peterson, B., Takeshita, Y., Matson, P.G., Crook, E.D., Kroeker, K.J.,
848 Gambi, M.C., Rivest, E.B., Frieder, C. a, Yu, P.C., Martz, T.R., 2011. High-
849 frequency dynamics of ocean pH: a multi-ecosystem comparison. *PLoS One* 6,
850 e28983. <https://doi.org/10.1371/journal.pone.0028983>

851 Hsu S. A., 1994. Determining the power-law wind-profile exponent under near-neutral
852 stability condidtions at sea. *J. Appl. Meteorol.* 33, 757–765.

853 Hu, X., Beseres Pollack, J., McCutcheon, M.R., Montagna, P. a., Ouyang, Z., 2015.

854 Long-term alkalinity decrease and acidification of estuaries in Northwestern Gulf of
855 Mexico. *Environ. Sci. Technol.* 49, 3401–3409. <https://doi.org/10.1021/es505945p>

856 Hu, X., Nuttall, M.F., Wang, H., Yao, H., Staryk, C.J., McCutcheon, M.R., Eckert, R.J.,
857 Embesi, J.A., Johnston, M.A., Hickerson, E.L., Schmahl, G.P., Manzello, D.,
858 Enochs, I.C., DiMarco, S., Barbero, L., 2018. Seasonal variability of carbonate
859 chemistry and decadal changes in waters of a marine sanctuary in the Northwestern
860 Gulf of Mexico. *Mar. Chem.* 205, 16–28.
861 <https://doi.org/10.1016/j.marchem.2018.07.006>

862 Jiang, L.-Q., Cai, W.-J., Wang, Y., 2008. A comparative study of carbon dioxide
863 degassing in river- and marine-dominated estuaries. *Limnol. Oceanogr.* 53, 2603–
864 2615. <https://doi.org/10.4319/lo.2008.53.6.2603>

865 Jiang, L.Q., Cai, W.J., Wang, Y., Bauer, J.E., 2013. Influence of terrestrial inputs on
866 continental shelf carbon dioxide. *Biogeosciences* 10, 839–849.
867 <https://doi.org/10.5194/bg-10-839-2013>

868 Kealoha, A.K., Shamberger, K.E.F., DiMarco, S.F., Thyng, K.M., Hetland, R.D.,
869 Manzello, D.P., Slowey, N.C., Enochs, I.C., 2020. Surface water CO₂ variability in
870 the Gulf of Mexico (1996–2017). *Sci. Rep.* 10, 1–13.
871 <https://doi.org/10.1038/s41598-020-68924-0>

872 Laruelle, G.G., Cai, W.-J., Hu, X., Gruber, N., Mackenzie, F.T., Regnier, P., 2018.
873 Continental shelves as a variable but increasing global sink for atmospheric carbon
874 dioxide. *Nat. Commun.* 9, 454. <https://doi.org/10.1038/s41467-017-02738-z>

875 Li, D., Chen, J., Ni, X., Wang, K., Zeng, D., Wang, B., Jin, H., Huang, D., Cai, W.J.,
876 2018. Effects of biological production and vertical mixing on sea surface *p*CO₂

877 variations in the Changjiang River Plume during early autumn: A buoy-based time
878 series study. *J. Geophys. Res. Ocean.* 123, 6156–6173.
879 <https://doi.org/10.1029/2017JC013740>

880 Liu, H., Zhang, Q., Katul, G.G., Cole, J.J., Chapin, F.S., MacIntyre, S., 2016. Large CO₂
881 effluxes at night and during synoptic weather events significantly contribute to CO₂
882 emissions from a reservoir. *Environ. Res. Lett.* 11, 1–8.
883 <https://doi.org/10.1088/1748-9326/11/6/064001>

884 Mathis, J.T., Pickart, R.S., Byrne, R.H., Mcneil, C.L., Moore, G.W.K., Juranek, L.W.,
885 Liu, X., Ma, J., Easley, R.A., Elliot, M.M., Cross, J.N., Reisdorph, S.C., Bahr, F.,
886 Morison, J., Lichendorf, T., Feely, R.A., 2012. Storm-induced upwelling of high
887 *p*CO₂ waters onto the continental shelf of the western Arctic Ocean and implications
888 for carbonate mineral saturation states. *Geophys. Res. Lett.* 39, 4–9.
889 <https://doi.org/10.1029/2012GL051574>

890 McCutcheon, M.R., Staryk, C.J., Hu, X., 2019. Characteristics of the carbonate system in
891 a semiarid estuary that experiences summertime hypoxia. *Estuaries and Coasts* 42,
892 1509–1523. <https://doi.org/10.1007/s12237-019-00588-0>

893 Millero, F.J., 2010. Carbonate constant for estuarine waters. *Mar. Freshw. Res.* 61, 139–
894 142.

895 Montagna, P.A., Brenner, J., Gibeaut, J., Morehead, S., 2011. Chapter 4: Coastal Impacts,
896 in: Jurgen Schmandt, Gerald R. North, and J.C. (Ed.), *The Impact of Global*
897 *Warming on Texas*. University of Texas Press, pp. 96–123.

898 Raymond, P.A., Cole, J.J., 2001. Gas exchange in rivers and estuaries: Choosing a gas
899 transfer velocity. *Estuaries* 24, 312–317. <https://doi.org/10.2307/1352954>

900 Robbins, L.L., Lisle, J.T., 2018. Regional acidification trends in florida shellfish
901 estuaries: a 20+ year look at pH, oxygen, temperature, and salinity. *Estuaries and*
902 *Coasts* 41, 1268–1281. <https://doi.org/10.1007/s12237-017-0353-8>

903 Sastri, A.R., Christian, J.R., Achterberg, E.P., Atamanchuk, D., Buck, J.J.H., Bresnahan,
904 P., Duke, P.J., Evans, W., Gonski, S.F., Johnson, B., Juniper, S.K., Mihaly, S.,
905 Miller, L.A., Morley, M., Murphy, D., Nakaoka, S.I., Ono, T., Parker, G., Simpson,
906 K., Tsunoda, T., 2019. Perspectives on in situ sensors for ocean acidification
907 research. *Front. Mar. Sci.* 6, 1–6. <https://doi.org/10.3389/fmars.2019.00653>

908 Schulz, K.G., Riebesell, U., 2013. Diurnal changes in seawater carbonate chemistry
909 speciation at increasing atmospheric carbon dioxide. *Mar. Biol.* 160, 1889–1899.
910 <https://doi.org/10.1007/s00227-012-1965-y>

911 Seim, H.E., Kjerfve, B., Sneed, J.E., 1987. Tides of Mississippi Sound and the adjacent
912 continental shelf. *Estuar. Coast. Shelf Sci.* 25, 143–156.
913 [https://doi.org/10.1016/0272-7714\(87\)90118-1](https://doi.org/10.1016/0272-7714(87)90118-1)

914 Semesi, I.S., Beer, S., Björk, M., 2009. Seagrass photosynthesis controls rates of
915 calcification and photosynthesis of calcareous macroalgae in a tropical seagrass
916 meadow. *Mar. Ecol. Prog. Ser.* 382, 41–47. <https://doi.org/10.3354/meps07973>

917 Shadwick E. H., Friedrichs M. A. M., Najjar R.G., De Meo, O. A., Friedman, J. R., Da,
918 F. Reay, W. G., 2019. High-Frequency CO₂ System Variability Over the Winter-to-
919 Spring Transition in a Coastal Plain Estuary. *J Geophys. Res. Ocean.* 124(11):
920 7626-7642. doi:10.1029/2019JC015246

921 Solis, R.S., Powell, G.L., 1999. Hydrography, Mixing Characteristics, and Residence
922 Time of Gulf of Mexico Estuaries, in: Bianchi, T.S., Pennock, J.R., Twilley, R.R.

923 (Eds.), *Biogeochemistry of Gulf of Mexico Estuaries*. John Wiley & Sons, Inc: New
924 York, pp. 29–61.

925 Takahashi, T., Sutherland, S.C., Sweeney, C., Poisson, A., Metzl, N., Tilbrook, B., Bates,
926 N., Wanninkhof, R., Feely, R.A., Sabine, C., Olafsson, J., Nojiri, Y., 2002. Global
927 sea-air CO₂ flux based on climatological surface ocean pCO₂, and seasonal
928 biological and temperature effects. *Deep. Res. Part II Top. Stud. Oceanogr.* 49,
929 1601–1622. [https://doi.org/10.1016/S0967-0645\(02\)00003-6](https://doi.org/10.1016/S0967-0645(02)00003-6)

930 Thurman, H. V., 1994. *Introductory Oceanography, Seventh Edition*. pp. 252–276.

931 Uppström, L.R., 1974. The boron/chlorinity ratio of deep-sea water from the Pacific
932 Ocean. *Deep. Res. Oceanogr. Abstr.* 21, 161–162. [https://doi.org/10.1016/0011-](https://doi.org/10.1016/0011-7471(74)90074-6)
933 [7471\(74\)90074-6](https://doi.org/10.1016/0011-7471(74)90074-6)

934 USGS, 2001. *Discharge Between San Antonio Bay and Aransas Bay, Southern Gulf*
935 *Coast, Texas, May-September 1999*.

936 Van Dam, B.R., Edson, J.B., Tobias, C., 2019. Parameterizing Air-Water Gas Exchange
937 in the Shallow, Microtidal New River Estuary. *J. Geophys. Res. Biogeosciences*
938 124, 2351–2363. <https://doi.org/10.1029/2018JG004908>

939 Waldbusser, G.G., Salisbury, J.E., 2014. Ocean acidification in the coastal zone from an
940 organism’s perspective: multiple system parameters, frequency domains, and
941 habitats. *Ann. Rev. Mar. Sci.* 6, 221–47. [https://doi.org/10.1146/annurev-marine-](https://doi.org/10.1146/annurev-marine-121211-172238)
942 [121211-172238](https://doi.org/10.1146/annurev-marine-121211-172238)

943 Wanninkhof, R., 1992. Relationship between wind speed and gas exchange. *J. Geophys.*
944 *Res.* 97, 7373–7382. <https://doi.org/10.1029/92JC00188>

945 Wanninkhof, R., Asher, W.E., Ho, D.T., Sweeney, C., McGillis, W.R., 2009. *Advances*

946 in quantifying air-sea gas exchange and environmental forcing. *Ann. Rev. Mar. Sci.*
947 1, 213–244. <https://doi.org/10.1146/annurev.marine.010908.163742>

948 Weiss, R.F., 1974. Carbon dioxide in water and seawater: the solubility of a non-ideal
949 gas. *Mar. Chem.* 2, 203–215.

950 Westfall, P.H., 1997. Multiple testing of general contrasts using logical constraints and
951 correlations. *J. Am. Stat. Assoc.* 92, 299–306.
952 <https://doi.org/10.1080/01621459.1997.10473627>

953 Yao, H., Hu, X., 2017. Responses of carbonate system and CO₂ flux to extended drought
954 and intense flooding in a semiarid subtropical estuary. *Limnol. Oceanogr.* 62, S112–
955 S130. <https://doi.org/10.1002/lno.10646>

956 Yao, H., McCutcheon, M.R., Staryk, C.J., Hu, X., 2020. Hydrologic controls on CO₂
957 chemistry and flux in subtropical lagoonal estuaries of the northwestern Gulf of
958 Mexico. *Limnol. Oceanogr.* 65, 1380–1398. <https://doi.org/10.1002/lno.11394>

959 Yates, K.K., Dufore, C., Smiley, N., Jackson, C., Halley, R.B., 2007. Diurnal variation of
960 oxygen and carbonate system parameters in Tampa Bay and Florida Bay. *Mar.*
961 *Chem.* 104, 110–124. <https://doi.org/10.1016/j.marchem.2006.12.008>

962